Ab Initio and DFT Study of the Formation Mechanisms of Polycyclic Aromatic Hydrocarbons: The Phenanthrene Synthesis from Biphenyl and Naphthalene

V. V. Kislov,† A. M. Mebel,* and S. H. Lin

Institute of Atomic and Molecular Sciences, Academia Sinica, P.O. Box 23−166, Taipei 10764, Taiwan

Received: February 11, 2002; In Final Form: April 19, 2002

Density functional B3LYP and ab initio CASSCF calculations with the 6-31G* basis set have been performed to investigate various mechanisms of phenanthrene formation from biphenyl and naphthalene. Three competitive reaction pathways contributing to the PAH formation in combustion have been studied. The first one (R1) involves abstraction of a hydrogen atom followed by acetylene addition, ring closure, and hydrogen loss (disproportionation). In the other two routes, the acetylene addition is followed by H loss (disproportionation), H abstraction, ring closure, and H addition (R2) or by H addition and H abstraction (can be replaced by an H shift), ring closure, and H loss (disproportionation) (R3). Additionally, a new mechanism of phenanthrene formation from biphenyl is suggested, which does not require a presence of H radicals and involves [4+2] acetylene cycloaddition to biphenyl followed by H_2 elimination. Although the highest barrier for this reaction is calculated to be ∼45 kcal/mol, it can take place at high temperatures. The reaction steps of hydrogen elimination from radical intermediates can occur not only by direct hydrogen loss but also by H disproportionations, which typically have much lower barriers and are highly exothermic. Equilibrium constants and rate constants for various reaction steps have been computed using the transition state theory and ab initio energies and molecular structural parameters and can be used for future kinetic modeling of the PAH formation networks. The calculations demonstrate that the proposed hydrogen abstraction−acetylene addition (HACA) scheme provides viable mechanisms for the PAH formation and growth in flames.

I. Introduction

Polycyclic aromatic hydrocarbons (PAH) and their active metabolites are known as the most toxic, mutagenic, and carcinogenic air pollutants,[1−4] present in our environment in the form of volatile particles or atmospheric aerosols.[5,6] The major sources of PAH emission are the processes of incomplete combustion used in transportation, manufacturing, and power generation: e.g., diesel and gasoline exhausts,[7−11] fuel oil or coal-fired electricity generating power plants,[12−14] residential heating using wood or coal combustion,[15,16] tobacco smoke,[17−19] burning of plastics,[20−23] and also uncontrolled forest fires and agricultural burning.[24−26] PAH were found as the nuclei to technologically important soot formation,[27−33] where a rise in soot production is strongly related to higher PAH levels. The synthesis of polyhedral fullerenes and fullerenic nanostructures also involves PAH intermediates.[34−39] Because of the great environmental health effects of PAH and their importance in different applications of combustion technology, a better understanding of reaction pathways leading to PAH is required.

Several mechanisms have been proposed for the formation of first species in the homologous series of PAH (i.e. naphthalene, phenanthrene, and pyrene). The first mechanism was suggested by Frenklach and co-workers[40−43] for acetylene combustion as the principal reaction pathway leading to naphthalene. This route involves two successive losses of ring hydrogen atoms followed by acetylene additions to the radical sites with subsequent ring closure reaction. A similar hydrogen abstraction−acetylene addition (HACA) scheme was introduced by Bittner and Howard[44] with the difference that a second acetylene molecule adds to the first one, and then the formation of the additional ring takes place by ring closure reaction of the second acetylene with the existing ring. Another HACA route, beginning with the formation of biphenyl and followed by the sequential addition of acetylene, was proposed by Frenklach and co-workers[45] in the benzene pyrolysis, where biphenyl was found to be the major product during fuel decomposition. The mechanism of PAH synthesis beginning from biphenyl is one of the subjects of the present paper.

A considerable attention has been paid to ab initio studies of some elementary reaction steps leading to the formation of the second aromatic ring adding to the first one;[46−51] however, the entire reaction network leading to PAH and soot has not been investigated so far by accurate ab initio calculations. Mebel et al.[46] used the G2M(rcc,MP2) method to calculate potential energy surface (PES) for the $C_6H_6 + H$ abstraction reaction, which represents the most important step in the HACA PAH synthesis. A quantum chemical study of PES for another important step in HACA PAH synthesis, the acetylene addition to the phenyl radical has been conducted by Yu et al.[47] using the BAC-MP4 method (bond-additivity corrected Møller−Plesset 4th order perturbation) in conjunction with experimental measurements of absolute rate constants. RRKM theory was applied to study the temperature and pressure dependence of the reaction rate constants using calculated thermochemical and molecular structure data. For the acetylene addition step $C_6H_5 + C_2H_2$ leading to the $C_6H_5C_2H_2$ intermediate (phenylvinyl radical), the calculated barrier and reaction heat were +3.1 and −45.2 kcal/mol, respectively. The $C_6H_5C_2H_2$ radical then can undergo a decomposition (hydrogen loss) giving phenylacetylene, $C_6H_5C_2H_2 \rightarrow C_6H_5C_2H + H$. This step was found to have a barrier of 41.2 kcal/mol and to be 38.2 kcal/mol

* To whom correspondence should be addressed.
† Permanent address: Institute of Solution Chemistry of Russian Academy of Sciences, Akademicheskaya St., 1, Ivanovo, 153045 Russia.

10.1021/jp020406t CCC: $22.00
Published on Web 06/05/2002

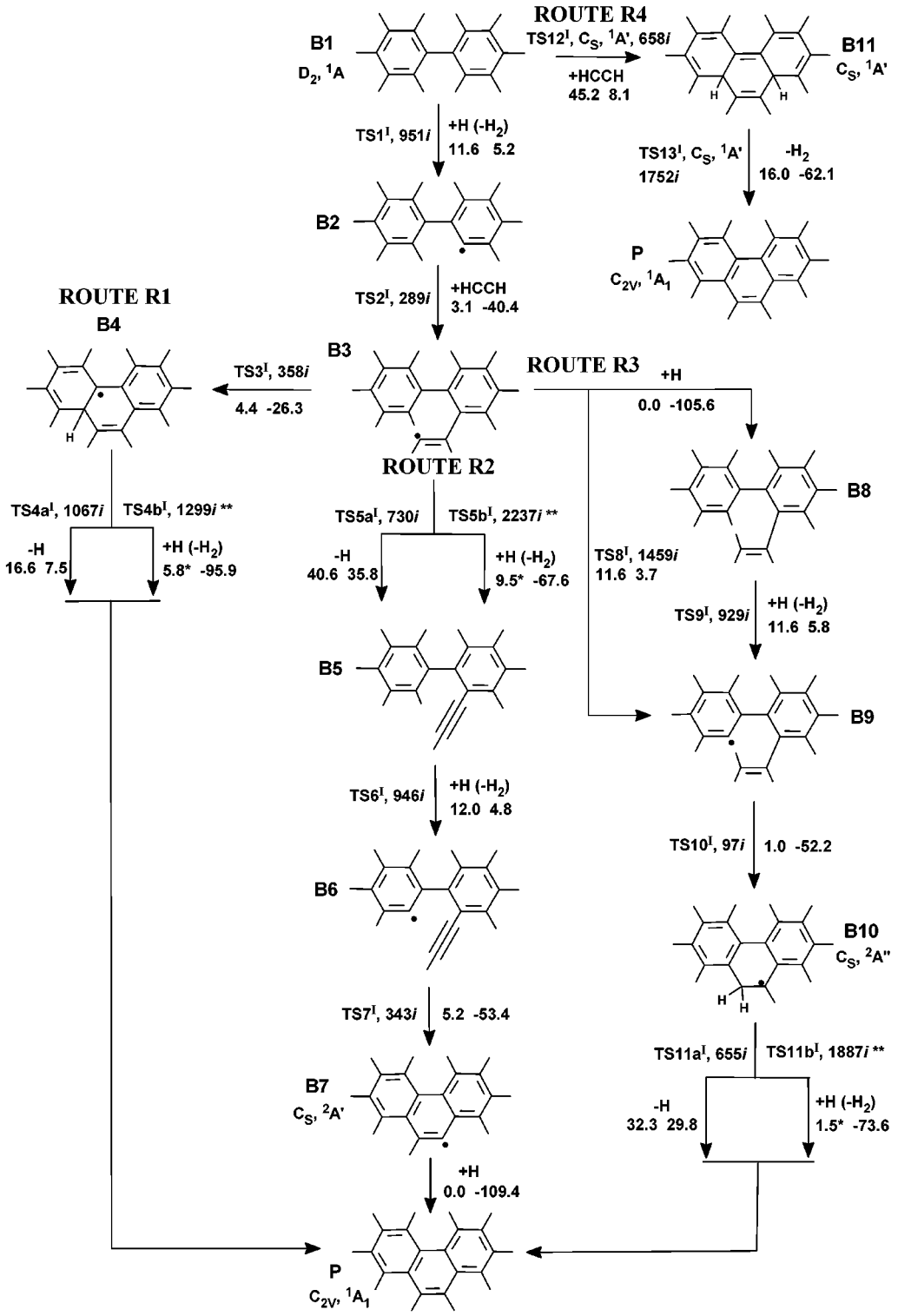

Figure 1. Reaction network **I** for the phenanthrene synthesis from biphenyl. The numbers given along reaction pathways represent barriers and heats of reaction (in kcal/mol) computed at the B3LYP/6-31G* level. Molecular symmetry groups and electronic states are also given for symmetric species. Asterisks mark the barriers calculated at the CASSCF/6-31G* level. Double asterisks label imaginary frequencies for transition states calculated at the UHF/6-31G* level.

endothermic, according to the BAC-MP4 calculations. On the other hand, the hydrogen migration in the $C_6H_5C_2H_2$ radical was studied by Frenklach and co-workers[48] at various levels of theory, who found the barrier of ~28−30 kcal/mol and concluded that the reaction rate is sufficiently fast to play a role in high-temperature aromatic chemistry. In a recent theoretical work, Bauschlicher and Ricca[49] calculated the reaction sequences leading to formation of the second aromatic ring (i.e., naphthalene) from benzene at the B3LYP/4-31G level. Both Frenklach and Bittner−Howard mechanisms were found to have low barriers and therefore to be equally probable. However, the calculated sequences were not complete, because the authors did not locate transition states for several important steps, in particular, for hydrogen elimination from the $C_6H_5C_2H_2$ intermediate to form phenylacetylene. Some other reactions were also missing in their calculations.

In this paper, we consider the dominant HACA reaction networks for the formation of phenanthrene (i.e., PAH contain-

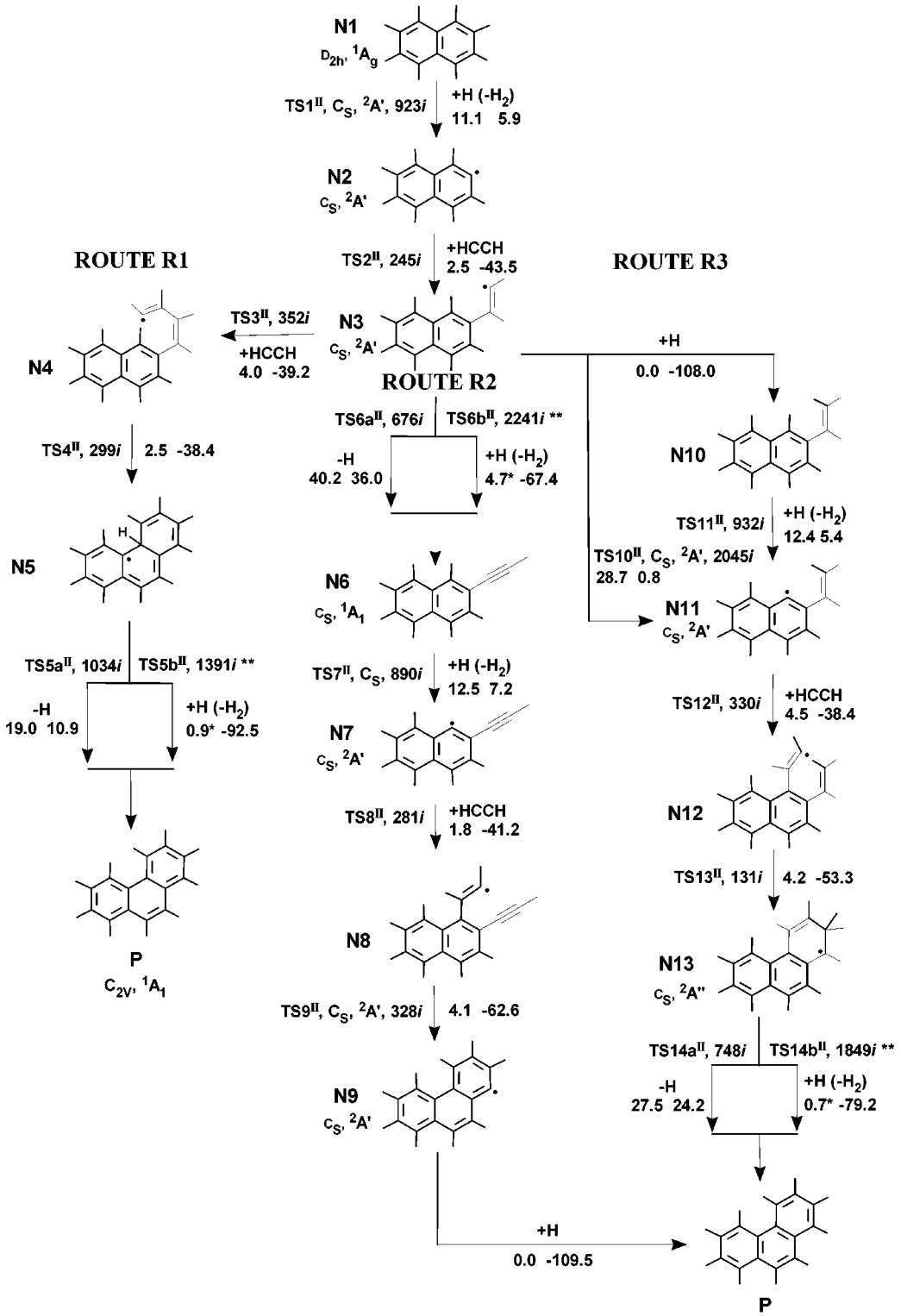

Figure 2. Reaction network **II** for the phenanthrene synthesis from naphthalene. The numbers given along reaction pathways represent barriers and heats of reaction (in kcal/mol) computed at the B3LYP/6-31G* level. Molecular symmetry groups and electronic states are also given for symmetric species. Asterisks mark the barriers calculated at the CASSCF/6-31G* level. Double asterisks label imaginary frequencies for transition states calculated at the UHF/6-31G* level.

ing three condensed aromatic rings), which is known as the precursor and substructure for the most of PAH exhibiting tumorogenic activity.[1−4] The first mechanism depicted in Figure 1 represents acetylene addition to biphenyl, giving phenanthrene, and was proposed previously as the dominant pathway leading to PAH in benzene combustion.[45] The second network shown in Figure 2 involves various HACA routes for the phenanthrene formation from naphthalene, originally suggested by Frenklach et al.[40−43] and Bittner and Howard[44] for the formation of the second aromatic ring. We also calculated additional reaction steps, not considered in the original mechanisms.

II. Computational Methods

The geometries for most intermediates and transition states were fully optimized using the hybrid density functional B3LYP method, i.e., the Becke's three-parameter nonlocal exchange

functional[52] with the nonlocal correlation functional of Lee, Yang, and Parr.[53] The 6-31G* basis set[54] was applied for all calculations. B3LYP/6-31G* geometry optimization was followed by analytical evaluation of harmonic frequencies at the same level of theory whereupon optimized structures were characterized as either local minima (no imaginary frequencies) or transition states (one imaginary frequency). Zero-point energy (ZPE) corrections were taken into account during calculation of barrier heights and heats of reactions using B3LYP/6-31G* frequencies without scaling.

The multireference CASSCF method[55] with four electrons distributed on six orbitals in the (4,6) active space has been employed for optimization and energy evaluation of open-shell singlet transition states **TS4b^{I}**, **TS5b^{I}**, and **TS11b^{I}** (reaction network **I**) and **TS5b^{II}**, **TS6b^{II}**, and **TS14b^{II}** (reaction network **II**). Before CASSCF optimization, geometries of these transition states were optimized at the UHF/6-31G* level and then the calculated structures were reoptimized at the CASSCF(4,6)/6-31G* level using UHF geometries and wave functions as the initial guess. Barriers for the reactions involving transition states mentioned above were also computed using the CASSCF method. We were unable to calculate CASSCF frequencies because this requires large computational costs; instead, harmonic frequencies of respective transition states were calculated at the UHF/6-31G* level, and ZPE corrections were evaluated using the HF frequencies scaled by a factor of 0.89. All of the calculations have been carried out using the Gaussian 98 program package.[56] The calculated barrier heights energies and heats of reactions are given in Figures 1 and 2 for reaction networks **I** and **II**, respectively, along with considered reaction pathways (electronic states and molecular symmetry point groups are also given for the species, which belong to a point group higher than C_1). Optimized geometries of all intermediates and transition states for the species involved in reaction networks **I** and **II** are shown in Figures S1 and S2 of the Supporting Information, respectively.

Reaction rate constants were estimated using the transition state theory[57] (TST) according to the following formula:

$$k = \left(\frac{RT}{p^{\varnothing}}\right)^{-\Delta n^{\ddagger}} \frac{k_B T}{h} e^{-\Delta G_0^{\ddagger}/RT}$$

where R is the Rydberg constant, k_B is the Boltzmann constant, h is the Planck constant, T and $p^{\varnothing}$ are the temperature and the standard pressure, respectively, $\Delta n^{\ddagger}$ is the change of the number of moles from reactants to the transition state, and $\Delta G_0^{\ddagger}$ is the change of the Gibbs free energy from reactants to the transition state. For the reactions involving hydrogen atoms, tunneling corrections (Q_{tun}) to the TST rate constants were computed using the Wigner formula:[58]

$$Q_{tun} = 1 - \frac{1}{24}\left(\frac{h\upsilon_S}{k_B T}\right)^2 (1 + k_B T/E_0)$$

where υ_S is the transition state imaginary frequency and E_0 is the barrier height including ZPE correction. All calculated rate constants are presented in Table 1. Equilibrium constants were computed using ab initio energies and molecular structural parameters as follows:

$$K_{eq} = \left(\frac{RT}{p^{\varnothing} N_A}\right)^{-\Delta n} e^{-\Delta G_0/RT}$$

where N_A is Avogadro constant, Δn is the change of the number of moles in the reaction, and ΔG_0 is the Gibbs free energy of the reaction. All calculated equilibrium constants are collected in Table 2. The Supporting Information provides calculated total energies for reactants and products, moments of inertia, and harmonic frequencies of all species involved.

III. Results and Discussion

1. Reaction Network I: Phenanthrene Synthesis from Biphenyl. The reaction network for the HACA phenanthrene synthesis from biphenyl is shown in Figure 1 along with computed barriers and heats of reactions. The network involves four most probable pathways (R1−R4), which can be suggested taking into account the results of the previous experimental study[45] and theoretical calcualtions.[49] In contrast to the phenanthrene synthesis from naphthalene or naphthalene synthesis from benzene, the synthesis starting from biphenyl requires only one acetylene addition step. Therefore, all routes proposed differ only by reaction steps leading to the ring closure. Because of that, three suggested routes (R1−R3) have the same two initial steps, abstraction of biphenyl's ortho-hydrogen atom (**B1**→**B2**) with subsequent acetylene addition to the radical site to form a radical intermediate **B3**. After that, the reaction sequence is branched into three routes leading to the ring closure via different intermediates.

The first route (R1), **B1** → **B2** → **B3** → **B4** → **P**, was originally proposed by Frenklach et al.[45] in their study of benzene combustion as the dominant route leading first to phenanthrene and then to pyrene. After the ring closure step giving the **B4** intermediate, the reaction sequence proceeds to phenanthrene via a loss of an "extra" hydrogen atom. The latter reaction occurs either directly (such pathway was considered by Frenklach et al.[45]) or by means of hydrogen disproportionation. The second route (R2), **B1** → **B2** → **B3** → **B5** → **B6** → **B7** → **P**, has two more steps and involves formation of biphenylacetylene $C_{14}H_{10}$ as an intermediate, with subsequent abstraction of another ortho-hydrogen atom giving a **B6** radical and a ring closure step. A similar pathway involving formation of phenylacetylene was calculated earlier[49] in the ab initio study of the Frenklach HACA naphthalene synthesis. The route R3, **B1** → **B2** → **B3** → **B8** → **B9** → **B10** → **P**, involves a 1,4-hydrogen shift (**B3** → **B9**) giving a radical **B9** (it can be also formed via production of intermediate **B8** followed by abstraction of the ortho-hydrogen atom), which then undergoes the ring closure giving the phenanthrene core with subsequent loss of an "extra" hydrogen atom. We also suggest an additional R4 route, **B1** → **B11** → **P**, which proceeds to phenanthrene without formation of radical species (i.e., does not involve hydrogen abstraction steps). In this pathway, the acetylene addition and ring closure occur in one reaction step (**B1** → **B11**) giving the phenanthrene core with two "extra" hydrogen atoms, and then the reaction proceeds to phenanthrene by elimination of the H_2 molecule.

Now let us discuss the calculated barriers, reaction heats, structures of intermediates, and transition states for the considered reaction pathways. The first reaction step **B1** → **B2**, the abstraction of ortho-hydrogen atom from biphenyl, was found to have a barrier of 11.6 kcal/mol. The reaction is 5.2 kcal/mol endothermic, and therefore, transition state **TS1^{I}** exhibits a late character. Our results agree well with available experimental and theoretical data for the C_6H_6 + H abstraction reaction.[46,49] The experimental reaction heat, 8.7 ± 0.6 kcal/mol,[46] is determined by the strength of the H−H bond in H_2 and the C−H bond in benzene. The activation energy and heat of the C_6H_6 + H reaction calculated by Mebel at al.[46] at the

TABLE 1: Calculated Rate Constants for All Reaction Steps Involved in Reaction Networks I and II

reaction	k							
T, K	300	500	1000	1500	2000	2500	3000	fitted expression
Hydrogen Abstraction (Disproportionation), $cm^3\ s^{-1}\ molecule^{-1}$								
B1+H → B2+H_2	4.35×10^{-19}	1.10×10^{-15}	7.06×10^{-13}	8.52×10^{-12}	3.45×10^{-11}	8.73×10^{-11}	1.71×10^{-10}	$3.14 \times 10^{-16}\ T^{1.87}\ \exp(-10270/RT)$
B4+H → P+H_2	1.25×10^{-15}	1.06×10^{-13}	1.05×10^{-11}	9.30×10^{-11}	3.55×10^{-10}	8.98×10^{-10}	1.79×10^{-9}	$3.19 \times 10^{-21}\ T^{3.48}\ \exp(-4166/RT)$
B3+H → B5+H_2	3.15×10^{-18}	2.14×10^{-15}	8.85×10^{-13}	1.27×10^{-11}	6.25×10^{-11}	1.86×10^{-10}	4.16×10^{-10}	$1.66 \times 10^{-21}\ T^{3.44}\ \exp(-7194/RT)$
B5+H → B6+H_2	5.57×10^{-20}	1.88×10^{-16}	1.50×10^{-13}	1.94×10^{-12}	8.18×10^{-12}	2.11×10^{-11}	4.21×10^{-11}	$8.06 \times 10^{-17}\ T^{1.87}\ \exp(-10696/RT)$
B8+H → B9+H_2	1.05×10^{-19}	2.74×10^{-16}	1.80×10^{-13}	2.19×10^{-12}	8.90×10^{-12}	2.25×10^{-11}	4.43×10^{-11}	$8.30 \times 10^{-17}\ T^{1.86}\ \exp(-10317/RT)$
B10+H → P+H_2	1.64×10^{-12}	5.85×10^{-12}	4.64×10^{-11}	1.71×10^{-10}	4.19×10^{-10}	8.14×10^{-10}	1.36×10^{-9}	$6.09 \times 10^{-21}\ T^{3.26}\ \exp(467/RT)$
N1+H → N2+H_2	1.10×10^{-18}	2.11×10^{-15}	1.11×10^{-12}	1.25×10^{-11}	4.92×10^{-11}	1.22×10^{-10}	2.36×10^{-10}	$3.71 \times 10^{-16}\ T^{1.88}\ \exp(-9853/RT)$
N5+H → P+H_2	6.67×10^{-12}	2.43×10^{-11}	2.70×10^{-10}	1.31×10^{-9}	4.00×10^{-9}	9.29×10^{-9}	1.81×10^{-8}	$3.06 \times 10^{-23}\ T^{4.23}\ \exp(1158/RT)$
N3+H → N6+H_2	2.58×10^{-14}	7.02×10^{-13}	2.30×10^{-11}	1.32×10^{-10}	4.07×10^{-10}	9.03×10^{-10}	1.65×10^{-9}	$3.88 \times 10^{-20}\ T^{3.12}\ \exp(-2615/RT)$
N6+H → N7+H_2	2.62×10^{-20}	1.31×10^{-16}	1.38×10^{-13}	1.95×10^{-12}	8.52×10^{-12}	2.25×10^{-11}	4.53×10^{-11}	$1.41 \times 10^{-16}\ T^{1.82}\ \exp(-11318/RT)$
N10+H → N11+H_2	1.50×10^{-20}	6.23×10^{-17}	5.65×10^{-14}	7.60×10^{-13}	3.25×10^{-12}	8.46×10^{-12}	1.69×10^{-11}	$5.04 \times 10^{-17}\ T^{1.82}\ \exp(-11033/RT)$
N13+H → P+H_2	1.37×10^{-11}	3.13×10^{-11}	1.73×10^{-10}	5.48×10^{-10}	1.24×10^{-9}	2.27×10^{-9}	3.66×10^{-9}	$3.94 \times 10^{-20}\ T^{3.14}\ \exp(1032/RT)$
H/H_2 Loss, s^{-1}								
B3 → B5+H	5.02×10^{-17}	6.76×10^{-5}	1.51×10^{5}	2.41×10^{8}	1.01×10^{10}	9.69×10^{10}	4.41×10^{11}	$4.31 \times 10^{14}\ \exp(-42633/RT)$
B4 → P+H	6.89	5.22×10^{5}	3.55×10^{9}	7.89×10^{10}	3.89×10^{11}	1.03×10^{12}	1.98×10^{12}	$3.02 \times 10^{13}\ \exp(-17479/RT)$
B10 → P+H	1.19×10^{-11}	4.60×10^{-2}	1.14×10^{6}	3.94×10^{8}	7.69×10^{9}	4.64×10^{10}	1.55×10^{11}	$3.54 \times 10^{13}\ \exp(-33735/RT)$
B11 → P+H_2	12.4	3.26×10^{5}	8.06×10^{8}	1.30×10^{10}	5.59×10^{10}	1.38×10^{11}	2.54×10^{11}	$2.79 \times 10^{12}\ \exp(-15680/RT)$
N5 → P+H	8.63×10^{-2}	3.35×10^{4}	7.80×10^{8}	2.61×10^{10}	1.58×10^{11}	4.72×10^{11}	9.88×10^{11}	$2.26 \times 10^{13}\ \exp(-19920/RT)$
N3 → N6+H	9.39×10^{-17}	9.63×10^{-5}	1.73×10^{5}	2.55×10^{8}	1.03×10^{10}	9.60×10^{10}	4.29×10^{11}	$3.94 \times 10^{14}\ \exp(-42200/RT)$
N13 → P+H	7.07×10^{-8}	10.3	2.13×10^{7}	3.21×10^{9}	4.12×10^{10}	1.94×10^{11}	5.48×10^{11}	$5.51 \times 10^{13}\ \exp(-28815/RT)$
Ring Closure/H Migration, s^{-1}								
B3 → B4	5.75×10^{8}	1.01×10^{10}	9.05×10^{10}	1.91×10^{11}	2.78×10^{11}	3.50×10^{11}	4.07×10^{11}	$8.27 \times 10^{11}\ \exp(-4348/RT)$
B6 → B7	4.11×10^{8}	1.36×10^{10}	1.92×10^{11}	4.67×10^{11}	7.32×10^{11}	9.60×10^{11}	1.15×10^{12}	$2.74 \times 10^{12}\ \exp(-5256/RT)$
B3 → B9	1.16×10^{4}	1.65×10^{7}	4.60×10^{9}	3.40×10^{10}	9.67×10^{10}	1.85×10^{11}	2.86×10^{11}	$1.60 \times 10^{12}\ \exp(-11254/RT)$
B9 → B10	4.69×10^{11}	1.03×10^{12}	1.90×10^{12}	2.34×10^{12}	2.61×10^{12}	2.78×10^{12}	2.90×10^{12}	$3.53 \times 10^{12}\ \exp(-1208/RT)$
N4 → N5	6.35×10^{9}	3.17×10^{10}	1.12×10^{11}	1.74×10^{11}	2.19×10^{11}	2.51×10^{11}	2.75×10^{11}	$4.07 \times 10^{11}\ \exp(-2498/RT)$
N8 → N9	1.23×10^{9}	1.84×10^{10}	1.45×10^{11}	2.92×10^{11}	4.16×10^{11}	5.16×10^{11}	5.95×10^{11}	$1.16 \times 10^{12}\ \exp(-4095/RT)$
N3 → N11	1.53×10^{-8}	2.14	3.06×10^{6}	3.90×10^{8}	4.62×10^{9}	2.08×10^{10}	5.72×10^{10}	$5.62 \times 10^{12}\ \exp(-28295/RT)$
N12 → N13	2.70×10^{9}	5.36×10^{10}	5.13×10^{11}	1.10×10^{12}	1.61×10^{12}	2.02×10^{12}	2.36×10^{12}	$4.96 \times 10^{12}\ \exp(-4486/RT)$
Acetylene Addition, $cm^3\ s^{-1}\ molecule^{-1}$								
B1+C_2H_2 → B11	1.65×10^{-47}	2.55×10^{-34}	4.10×10^{-24}	1.62×10^{-20}	1.27×10^{-18}	1.99×10^{-17}	1.36×10^{-16}	$1.67 \times 10^{-13}\ \exp(-47004/RT)$ $3.19 \times 10^{-22}\ T^{2.52}\ \exp(-43285/RT)$
B2+C_2H_2 → B3	4.95×10^{-16}	8.79×10^{-15}	1.64×10^{-13}	6.75×10^{-13}	1.70×10^{-12}	3.36×10^{-12}	5.75×10^{-12}	$1.76 \times 10^{-20}\ T^{2.50}\ \exp(-2383/RT)$
N2+C_2H_2 → N3	9.86×10^{-15}	1.33×10^{-13}	2.06×10^{-12}	8.18×10^{-12}	2.10×10^{-11}	4.32×10^{-11}	7.80×10^{-11}	$2.52 \times 10^{-20}\ T^{2.76}\ \exp(-1705/RT)$
N3+C_2H_2 → N4	2.57×10^{-16}	7.55×10^{-15}	1.98×10^{-13}	9.06×10^{-13}	2.40×10^{-12}	4.89×10^{-12}	8.54×10^{-12}	$4.08 \times 10^{-20}\ T^{2.46}\ \exp(-3140/RT)$
N7+C_2H_2 → N8	7.43×10^{-15}	5.64×10^{-14}	5.57×10^{-13}	1.86×10^{-12}	4.22×10^{-12}	7.83×10^{-12}	1.29×10^{-11}	$2.60 \times 10^{-20}\ T^{2.52}\ \exp(-1089/RT)$
N11+C_2H_2 → N12	3.08×10^{-17}	1.30×10^{-15}	4.67×10^{-14}	2.39×10^{-13}	6.71×10^{-13}	1.42×10^{-12}	2.54×10^{-12}	$8.05 \times 10^{-21}\ T^{2.52}\ \exp(-3652/RT)$

G2M(rcc,MP2) level are 19.9 and 11.1 kcal/mol, respectively. For the same reaction, Bauschlicher at al.[49] found the barrier height and heat of reaction to be 11.5 and 6.9 kcal/mol, respectively, at the B3LYP/4-31G level, substantially lower than the G2M(rcc,MP2) predictions of Mebel et al. This indicates that the barrier height at **TS1^{I}** may be underestimated by the B3LYP calculations. The hydrogen abstraction transition state **TS1^{I}** has no symmetry, like most of the intermediates and transition states in the considered network. The critical CHH fragment is linear and lies in the plane of the aromatic ring. Its geometry and imaginary frequency are close to those in the corresponding transition state for the C_6H_6 + H reaction. In fact, our calculated C−H and H−H bond lengths are 1.48 and 0.86 Å, respectively, whereas the corresponding values for the C_6H_6 + H reaction are 1.49 and 0.85 Å at the MP2/6-31G* level and 1.48 and 0.85 Å at the B3LYP/6-31G** level.[46] In **TS1^{I}**, the C−H bond elongates by 0.4 Å as compared to a regular C−H bond in biphenyl, and the H−H bond, which is being formed, is 0.1 Å longer as compared to that in the H_2 molecule. Because **TS1^{I}** has a late character, the geometry of the $C_{12}H_9$ fragment in this transition state is close to that in the biphenyl radical **B2**.

The next step (**B2 → B3**) is the acetylene addition to the radical site. This reaction has a low barrier of 3.1 kcal/mol and is exothermic by 40.4 kcal/mol. Our calculated barrier height and reaction heat are close to those obtained by Yu et al.[47] at the BAC-MP4 level (+3.1 and −45.2 kcal/mol, respectively) and Bauschlicher at al.[49] at the B3LYP/4-31G level (+2.5 and −42.2 kcal/mol, respectively) for the acetylene addition to the phenyl radical. Transition state **TS2^{I}** exhibits an early character (reactant-like structure); the forming C−C bond is elongated by 0.9 Å in comparison with that in **B3** and the geometry of the biphenyl moiety is close to that in **B2**. The acetylene fragment in **TS2^{I}** has a nonlinear structure; otherwise, its geometry is similar to that for the acetylene molecule; the C−C and C−H bonds are elongated only by 0.015 and 0.003 Å, respectively, as compared with respective bonds in C_2H_2. The twisting angle τ between two aromatic rings of 38.0° in **TS2^{I}** is practically the same as that in biphenyl (38.4°) as well as in **TS1^{I}** (38.2°). The **B3** intermediate, which plays a key role in the considered network, has the geometry of the biphenyl moiety similar to that in biphenyl itself, except the twisting angle τ, which is about 20° larger in **B3**, probably because of the electrostatic repulsion between the acetylene fragment and hydrogen atoms of the second aromatic ring. The acetylene fragment in **B3** lies almost in the plane of the benzene ring.

After the formation of **B3**, the reaction network is branched into three different channels, R1−R3, with all of them leading to the ring closure and formation of the phenanthrene core. For the R1 channel, the ring closure step **B3 → B4** takes place immediately after the acetylene addition to biphenyl radical (**B2 → B3)** giving a **B4** intermediate, which has three fused aromatic

TABLE 2: Calculated Equilibrium Constants for All Reaction Steps Involved in Reaction Networks I and II

reaction	K_{eq}						
T, K	300	500	1000	1500	2000	2500	3000
Hydrogen Abstraction (Disproportionation), Dimensionless							
B1+H → B2+H_2	5.04×10^{-3}	0.261	5.27	13.1	19.3	23.2	25.4
B4+H → P+H_2	4.69×10^{69}	5.78×10^{41}	5.49×10^{20}	4.47×10^{13}	1.15×10^{10}	7.66×10^{7}	2.61×10^{6}
B3+H → B5+H_2	1.44×10^{49}	4.04×10^{29}	8.52×10^{14}	9.49×10^{9}	2.89×10^{7}	8.45×10^{5}	7.76×10^{4}
B5+H → B6+H_2	2.39×10^{-3}	9.34×10^{-2}	1.52	3.51	4.97	5.84	6.32
B8+H → B9+H_2	1.74×10^{4}	2.18×10^{4}	3.31×10^{4}	4.45×10^{4}	5.60×10^{4}	6.76×10^{4}	7.92×10^{4}
B10+H → P+H_2	1.50×10^{53}	5.67×10^{31}	4.19×10^{15}	1.50×10^{10}	2.57×10^{7}	5.33×10^{5}	3.89×10^{4}
N1+H → N2+H_2	1.06×10^{-3}	8.53×10^{-2}	2.40	6.67	10.3	12.9	14.4
N5+H → P+H_2	1.11×10^{67}	1.35×10^{40}	7.18×10^{19}	1.04×10^{13}	3.58×10^{9}	2.83×10^{7}	1.08×10^{6}
N3+H → N6+H_2	1.05×10^{49}	3.27×10^{29}	7.42×10^{14}	8.47×10^{9}	2.61×10^{7}	7.70×10^{5}	7.10×10^{4}
N6+H → N7+H_2	3.28×10^{-5}	6.29×10^{-3}	0.332	1.13	1.93	2.53	2.95
N10+H → N11+H_2	3.10×10^{-4}	1.74×10^{-2}	0.367	0.924	1.36	1.64	1.80
N13+H → P+H_2	3.23×10^{57}	2.87×10^{34}	1.24×10^{17}	1.71×10^{11}	1.82×10^{8}	2.83×10^{6}	1.70×10^{5}
H/H_2 Loss, molecule cm^{-3}							
B4 → P+H	1.57×10^{18}	3.52×10^{20}	1.91×10^{22}	6.42×10^{22}	1.08×10^{23}	1.38×10^{23}	1.56×10^{23}
B3 → B5+H	4.83×10^{-3}	2.46×10^{8}	2.97×10^{16}	1.36×10^{19}	2.69×10^{20}	1.52×10^{21}	4.62×10^{21}
B10 → P+H	50.3	3.46×10^{10}	1.46×10^{17}	2.15×10^{19}	2.40×10^{20}	9.60×10^{20}	2.32×10^{21}
B11 → P+H_2	2.38×10^{69}	3.49×10^{51}	1.34×10^{38}	3.57×10^{33}	1.56×10^{31}	5.37×10^{29}	5.27×10^{28}
N5 → P+H	3.71×10^{15}	8.20×10^{18}	2.50×10^{21}	1.49×10^{22}	3.34×10^{22}	5.09×10^{22}	6.46×10^{22}
N3 → N6+H	3.50×10^{-3}	1.99×10^{8}	2.59×10^{16}	1.22×10^{19}	2.43×10^{20}	1.39×10^{21}	4.23×10^{21}
N13 → P+H	1.08×10^{6}	1.75×10^{13}	4.33×10^{18}	2.45×10^{20}	1.70×10^{21}	5.09×10^{21}	1.01×10^{22}
Ring Closure/H Migration, Dimensionless							
B3 → B4	1.38×10^{18}	1.56×10^{10}	1.40×10^{4}	1.30×10^{2}	12.6	3.09	1.21
B6 → B7	4.41×10^{37}	4.82×10^{21}	3.53×10^{9}	2.93×10^{5}	2.64×10^{4}	1.56×10^{2}	23.6
B3 → B9	2.28×10^{-3}	2.72×10^{-2}	0.164	0.291	0.386	0.457	0.510
B9 → B10	1.60×10^{37}	5.28×10^{21}	1.06×10^{10}	1.29×10^{6}	1.42×10^{4}	9.52×10^{2}	1.57×10^{2}
N4 → N5	5.05×10^{26}	1.56×10^{15}	2.93×10^{6}	3.48×10^{3}	1.19×10^{2}	15.8	4.10
N8 → N9	1.70×10^{44}	2.81×10^{25}	1.32×10^{11}	1.94×10^{6}	7.31×10^{3}	2.55×10^{2}	27.2
N3 → N11	0.325	0.546	0.745	0.803	0.827	0.839	0.846
N12 → N13	9.53×10^{37}	1.26×10^{22}	1.11×10^{10}	9.99×10^{5}	9.38×10^{3}	5.69×10^{2}	87.8
Acetylene/H Addition, cm^3 $molecule^{-1}$							
B2+C_2H_2 → B3	4.15×10^{2}	5.80×10^{-10}	1.09×10^{-18}	1.92×10^{-21}	9.87×10^{-23}	1.89×10^{-23}	6.82×10^{-24}
B7+H → P	1.27×10^{55}	8.12×10^{22}	4.82×10^{-2}	4.16×10^{-10}	4.11×10^{-14}	1.71×10^{-16}	4.59×10^{-18}
B3+H → B8	2.74×10^{52}	2.26×10^{21}	8.62×10^{-3}	1.35×10^{-10}	1.79×10^{-14}	8.84×10^{-17}	2.66×10^{-18}
B1+C_2H_2 → B11	1.91×10^{-33}	2.38×10^{-31}	1.15×10^{-29}	5.89×10^{-29}	1.65×10^{-28}	3.47×10^{-28}	6.22×10^{-28}
N2+C_2H_2 → N3	1.26×10^{5}	2.30×10^{-8}	9.36×10^{-18}	9.88×10^{-21}	3.94×10^{-22}	6.47×10^{-23}	2.11×10^{-23}
N3+C_2H_2 → N4	2.02×10^{2}	5.40×10^{-10}	1.41×10^{-18}	2.66×10^{-21}	1.41×10^{-22}	2.73×10^{-23}	9.94×10^{-24}
N7+C_2H_2 → N8	3.76×10^{3}	3.48×10^{-9}	4.95×10^{-18}	8.01×10^{-21}	3.96×10^{-22}	7.40×10^{-23}	2.63×10^{-23}
N9+H → P	1.54×10^{55}	9.27×10^{22}	5.30×10^{-2}	4.52×10^{-10}	4.44×10^{-14}	1.84×10^{-16}	4.93×10^{-18}
N3+H → N10	3.13×10^{54}	5.15×10^{22}	5.81×10^{-2}	6.05×10^{-10}	6.51×10^{-14}	2.84×10^{-16}	7.88×10^{-18}
N11+C_2H_2 → N12	11.3	5.77×10^{-11}	2.88×10^{-19}	7.05×10^{-22}	4.28×10^{-23}	9.03×10^{-24}	3.49×10^{-24}

rings. In the case of R2 and R3 channels, the ring closure is preceded by several steps. For R2, we see a hydrogen elimination from the acetylene fragment, **B3 → B5**, giving biphenylacetylene **B5** (this step has two channels, which correspond either to the H disproportionation by free H radical or direct H loss) followed by the hydrogen abstraction from another aromatic ring, **B5 → B6**, giving intermediate **B6** with a radical site. The former step has the barrier of 12 kcal/mol and reaction heat of 4.8 kcal/mol very close to those for the **B1 → B2** hydrogen abstraction reaction. Also, the CHH fragment structure and imaginary frequency in **TS7^{I}** are close to those in **TS1^{I}**. The R3 route proceeds via the formation of a radical **B9** by two possible channels, via the formation of intermediate **B8** (H addition, **B3 → B8**, has no barrier) followed by the hydrogen abstraction, **B8 → B9**, or in one step, by the 1,6-hydrogen shift, **B3 → B9**. Both channels seem equally probable because the **B8 → B9** and **B3 → B9** steps have almost the same barrier and reaction endothermicity. We can see that all H abstraction steps from the singlet molecules involving ring hydrogen atoms (i.e., **B1 → B2**, **B5 → B6**, and **B8 → B9**) have similar barriers (∼12 kcal/mol), heats of reaction (about 6 kcal/mol), as well as transition state structures. As discussed above, these values are also close to those found for the hydrogen abstraction from benzene.[46,49] For the 1,6-hydrogen shift channel via **TS8^{I}**, our calculated barrier of 11.6 kcal/mol is 16.9 kcal/mol lower, and the reaction heat of 3.7 kcal/mol is 2.6 kcal/mol higher than the respective values for the 1,4-hydrogen shift in the phenylacetylene radical $C_6H_5-C_2H_2$ obtained by Bauschlicher et al.[49] at the B3LYP/4-31G level.

All ring closure steps in the biphenyl → phenanthrene reaction network exhibit low barriers (about 5 kcal/mol) and are strongly exothermic (25−50 kcal/mol). Therefore, transition states **TS3^{I}**, **TS7^{I}**, and **TS10^{I}** for these steps should have an early, reactant-like character. The forming C−C bond in the transition states is still long, 0.75 (**TS3^{I}**), 0.98 (**TS7^{I}**), and 1.56 Å (**TS10^{I}**) longer as compared to those in the products, **B4**, **B7**, and **P**, respectively. The barrier at **TS10^{I}** is very low, ∼1.0 kcal/mol, indicating that the **B9** intermediate is unstable and rearranges to **B10** immediately. For the **B3 → B4** ring closure step, the calculated barrier (4.4 kcal/mol) and heat of reaction (−26.3 kcal/mol) closely agree with respective values obtained by Bauschlicher et al.[49] at the B3LYP/4-31G level for the ring closure step in the Bittner−Howard naphthalene synthesis. In their case, the ring closure leads to an intermediate with an "extra" hydrogen similar to **B4** and the barrier, and reaction exothermicities are 7.3 and 23.6 kcal/mol, respectively.

Now let us discuss the hydrogen elimination steps **B4 → P**, **B3 → B5**, and **B10 → P**. From our point of view, these reactions

are most interesting in the considered network because, besides direct H loss, they can occur by disproportionation of a hydrogen atom from radical species, which can play an important role in combustion chemistry. We were unable to optimize transition state structures **TS4b^{I}**, **TS5b^{I}**, and **TS11b^{I}** for the hydrogen disproportionation channel using the B3LYP method; the calculations did not converge during transition state optimization. In the disproportionation reactions, the wave functions change their character from an open shell singlet in the reactants to a closed shell singlet in products. Such a situation is difficult to describe by single reference methods and by UB3LYP calculations in particular, despite the fact that this method is remarkably stable for radical species and largely removes spin contamination. The failure in the transition state search may indicate that either the barrier does not exist or the UB3LYP method does not properly describe the wave function in the transition state vicinity. Therefore, we tried to calculate transition state structures **TS4b^{I}**, **TS5b^{I}**, and **TS11b^{I}** using the CASSCF(4,6)/6-31G* method. Additionally, we reoptimized geometries and recalculated total energies of the **B4**, **B3**, and **B10** radicals using the same CASSCF method. The results show that the barriers for the disproportionation reactions do exist at the CASSCF level, although their heights may be somewhat overestimated as compared to the B3LYP results.[48] A quantitative comparison can be done only if the whole set of calculations is performed at the same level of theory which should be able to describe properly all reactions in the network, for example, CASMP2//CASSCF. However, for the system under consideration, such an approach is unfeasible at the moment.

According to our results, the H disproportionation mechanism is more favorable energetically for the **B4** → **P**, **B3** → **B5**, and **B10** → **P** reactions than the direct H loss mechanism; the former channel has much lower barrier and is strongly exothermic, whereas the H loss channel is endothermic by few tens of a kcal/mol. The preference of the hydrogen disproportionation mechanism has an obvious explanation, namely, in this mechanism two radicals react to give two singlet molecules, whereas in the case of the direct hydrogen loss, the products are an H radical and a closed shell molecule. The lowest barrier (of only 1.5 kcal/mol) is found for the **B10** → **P** step, whereas for the **B4** → **P** and **B3** → **B5** reactions, the barriers are higher, 5.8 and 9.5 kcal/mol, respectively. The **B4** → **P**, **B3** → **B5**, and **B10** → **P** reaction steps are highly exothermic, 95.9, 67.6, and 73.6 kcal/mol, respectively. Interestingly, our calculated heat for the **B3** → **B5** reaction (−67.6 kcal/mol) is close to that (−64.6 kcal/mol) obtained by Bauschlicher et al.[49] for the $C_6H_5C_2H_2$ + H reaction at the B3LYP/4-31G level. According to our CASSCF computations, transition states **TS4b^{I}**, **TS5b^{I}**, and **TS11b^{I}** have an early character, in accord with the fact that the corresponding reactions are exothermic. The forming H−H bond is 1.19 (**TS4b^{I}**), 0.51 (**TS5b^{I}**), and 0.65 Å (**TS11b^{I}**) longer as compared to the H_2 bond length, whereas the breaking C−H bond is stretched only by 0.06 and 0.05 Å in **TS5b^{I}** and **TS11b^{I}**, as compared to the reactant structures **B3** and **B10**. In transition state **TS4b^{I}**, we found almost the same bond length for the critical C−H bond as in the reactant **B4**.

In contrast to the H disproportionation channels, we were able to optimize transition states and calculate barriers for the H loss channels using the UB3LYP method for doublet electronic states. In all cases considered here, direct hydrogen loss requires much higher barriers as compared to the respective hydrogen disproportionation channel. Moreover, the hydrogen loss **B4** → **P**, **B3** → **B5**, and **B10** → **P** reactions are endothermic, with late transition states **TS4a^{I}**, **TS5a^{I}**, and **TS11a^{I}**. The breaking C−H bond in these transition states is elongated by 0.58 (**TS4a^{I}**), 0.83 (**TS5a^{I}**), and 0.87 Å (**TS11a^{I}**) as compared to those in the reactants, **B4**, **B3**, and **B10**, respectively. The heats of the **B4** → **P** and **B3** → **B5** hydrogen loss channels are in good agreement with those calculated by Bauschlicher at al.[49] for similar steps in the HACA naphthalene synthesis. Namely, they found the heats of reaction of 34.8 and 2.9 kcal/mol for the hydrogen loss from the $C_6H_5-C_2H_2$ radical (hydrogen elimination from the acetylene fragment) and for hydrogen loss from $C_{10}H_9$ (phenanthrene with an 'extra' hydrogen), respectively. Our values for the **B4** → **P** and **B3** → **B5** steps are only slightly higher, 35.8 and 7.5 kcal/mol, respectively. The computed barrier of 41.2 kcal/mol and reaction heat of 38.2 kcal/mol obtained by Yu et al.[47] at the BAC-MP4 level for the $C_6H_5C_2H_2$ → $C_6H_5C_2H$ + H hydrogen loss step are also close to our B3LYP/6-31G* calculated values for the similar hydrogen loss channel in **B3** → **B5** reaction.

Although the disproportionation pathways have much lower barriers than the direct hydrogen loss, they have to compete with recombination of the radical intermediates with the hydrogen atom. The recombination process where H adds to the radical site normally does not have any barrier and therefore is expected to be faster than the disproportionation reaction, at least, when the temperature is not very high. Earlier,[50] we calculated and compared reaction rate constants for recombination and disproportionation channels of the C_6H_5 + H reaction and found that the disproportionation process becomes more important than recombination at $T > 2000$ K. Therefore, both disproportionation and unimolecular H loss from radical intermediates have to be considered in kinetic models of PAH formation.

Finally, the R4 route consists of only two steps, direct acetylene addition to biphenyl, **B1** → **B11**, followed by elimination of molecular hydrogen, **B1** → **P**. The **B1** → **B11** step requires a relatively high barrier of 45.2 kcal/mol; therefore, the R4 route should be less probable as compared to the other routes in the network. The reaction proceeds without formation of radicals and requires higher activation energy than for the reactions involving radicals. However, such a process may occur in special conditions (e.g., at higher temperatures and when the concentration of free radicals is low) and should be taken into account in kinetic modeling. The first reaction step, **B1** → **B11**, can be characterized as a [4+2] cycloaddition or a Diels−Alder type reaction. Two new C−C bonds between carbon atoms of acetylene and biphenyl are formed simultaneously resulting in the third carbon ring. Interestingly, a similar reaction of *cis*-butadiene and acetylene exhibits a twice lower barrier of ∼22 kcal/mol.[59] However, the $H_2CCHCHCH_2$ + C_2H_2 reaction is 56 kcal/mol exothermic,[59] whereas the **B1** → **B11** step is 8.1 kcal/mol endothermic. **TS12^{I}** is C_s-symmetric and has a loose character. The forming C−C bonds are 0.54 and 0.63 Å longer than those in **B11** and phenanthrene, respectively. The geometry of the acetylene fragment in **TS12^{I}** is slightly deformed as compared to the acetylene molecule; the C−C and C−H bonds are elongated only by 0.05 and 0.01 Å, respectively, but the CHH angle, 145°, is far from the linear arrangement. The addition of acetylene slightly deforms the biphenyl moiety in **TS12^{I}**, which is found to have a more planar structure, with the twisting angle between two aromatic rings close to 0° vs 38° in biphenyl. However, the biphenyl fragment in **TS12^{I}** remains nonplanar; it is slightly bent along the $C_{Ph}-C_{Ph}$ bond. The **B11** intermediate and **TS13^{I}** also belong to the C_s point group. Interestingly, the **B11** → **P** reaction (loss of molecular hydrogen) exhibits a relatively small barrier of 16 kcal/mol that

is close to the barriers for hydrogen abstraction reactions (for example, 11.6 kcal/mol for **B1→B2**). On the other hand, the reaction is highly exothermic by 62.1 kcal/mol, so the heat of reaction is much higher than for a typical abstraction reaction. As a result, **TS13^{I}** has an early character. One can see that in **B11** and **TS13^{I}** the C−C bond in the acetylene fragment is parallel to the C_{Ph}−C_{Ph} bond of the biphenyl fragment, and C−H bonds of extra hydrogens are almost perpendicular to the plains of respective aromatic rings. The critical H−H bond in **TS13^{I}** is 0.38 Å longer as compared to that in the hydrogen molecule, and the breaking C−H bonds are elongated by 0.27 Å relative to those in the **B11** radical.

2. Reaction Network II: Phenanthrene Synthesis from Naphthalene. The calculated reaction network for the HACA phenanthrene synthesis from naphthalene is summarized in Figure 2. Computed barriers, heats of reactions, electronic states, and molecular symmetry groups are also given. This network is similar to that for the HACA mechanism of the naphthalene formation from benzene investigated by Bauschlicher at al.[49] at the B3LYP/4-31G level. The R1 and R2 channels represent the Bittner−Howard[44] and Frenklach[40−43] mechanisms of the PAH synthesis, respectively, whereas the route R3 was suggested by Bauschlicher et al.[49] The difference between the Bittner−Howard and Frenklach mechanisms is that the former involves addition of the second acetylene molecule to the first one, whereas in the latter, both acetylene molecules add to the aromatic ring. The third route (R3) is similar to the Frenklach mechanism with the difference that a C_2H_3 fragment and a C_2H_2 fragment containing a radical site are involved in the ring closure step. All proposed mechanisms start from the abstraction of a β-hydrogen atom in naphthalene followed by acetylene addition to the radical site giving the **N3** intermediate. Then, the reaction mechanism is branched into three different routes eventually leading to a ring closure step, which gives the phenanthrene core. We found that all considered pathways have low barriers and are therefore feasible during the PAH formation in combustion processes.

The **N1 → N2**, **N6 → N7** and **N10 → N11** steps correspond to abstraction of hydrogen atoms from the α or β positions in carbon rings of the naphthalene moiety and involve singlet PAH intermediates. All the three steps have similar barrier heights (within 11−13 kcal/mol) and heat of reactions (within 5−7 kcal/mol), as well as geometries of respective transition states **TS1^{II}**, **TS7^{II}**, and **TS11^{II}** (see Figure 2). In fact, the computed lengths for the critical breaking C−H and forming H−H bonds are within 1.49−1.50 and 0.85−0.86 Å, respectively. In contrast to **TS1^{II}** and **TS7^{II}**, the CHH fragment in **TS11^{II}** was found to have a slightly nonlinear structure with the CHH angle of 176°, most likely because of steric repulsion between the adjacent CHH and C_2H_3 fragments. Because the abstraction reactions are about 5−7 kcal/mol endothermic, the transition states exhibit a late character. The C−H bond distances are elongated by ∼0.4 Å as compared to the respective C−H bonds in naphthalene, whereas the forming H−H bond is 0.10−0.15 Å longer as compared to that in the H_2 molecule. The transition states **TS1^{II}** and **TS7^{II}** belong to the C_s point group (planar structures), whereas **TS11^{II}** has no symmetry, because the C_2H_3 fragment lies out of the aromatic ring plane. The results of our calculations are in a relatively good accord with the respective energetic parameters for the C_6H_6 + H abstraction reaction.[46,49] Indeed, the experimental heat of the C_6H_6 + H reaction as determined from the strength of the H−H bond in H_2 and C−H bond in benzene is 8.7 ± 0.6 kcal/mol,[46] the barrier height and heat of reaction calculated at the B3LYP/4-31G level are 11.5 and 6.9 kcal/mol, respectively,[49] but somewhat higher values (19.9 and 11.1 kcal/mol, respectively) were obtained using more accurate G2M(rcc,MP2) calculations. The optimized C−H and H−H bond lengths for **TS1^{II}**, **TS7^{II}**, and **TS11^{II}** slightly (within ∼0.01 Å) differ from those for the transition state of C_6H_6 + H, 1.49 and 0.85 Å at the MP2/6-31G* level and 1.48 and 0.85 Å at B3LYP/6-31G**.[46]

The acetylene addition steps usually following hydrogen abstraction are **N2 → N3**, **N3 → N4**, **N7 → N8**, and **N11 → N12**. Among those, only **N3 → N4** represents acetylene addition to another acetylene fragment, whereas **N2 → N3**, **N7 → N8**, and **N11 → N12** correspond to the acetylene addition to the aromatic ring. All of the addition steps have low barriers in the 1.8−4.5 kcal/mol range and are exothermic by ∼40 kcal/mol. Similar values of +2.5 and −42.2 kcal/mol for the barrier and heat of reaction, respectively, were found for the acetylene addition to the phenyl radical at the B3LYP/4-31G level.[49] Because the reactions are exothermic, transition states **TS2^{II}**, **TS3^{II}**, **TS8^{II}**, and **TS12^{II}** have an early, reactant-like character; the forming C−C bond is quite long and elongated by about 0.9 Å as compared to those in the products, **N3**, **N4**, **N8**, and **N12**. The geometry of the adding acetylene moiety is only slightly changed in comparison to isolated acetylene. Although the acetylene fragment is found to be nonlinear in all transition states, the C−C bond is stretched only by about 0.02 Å, and the C−H bonds are elongated by about 0.005 Å with respect to those in C_2H_2. All acetylene addition transition states have no symmetry with the adding C_2H_2 molecule usually lying out of the naphthalene moiety plane, whereas some reactants and products (**N2**, **N3**, and **N11**) of the acetylene addition reactions are planar.

All calculated ring closure reactions, **N4 → N5**, **N8 → N9**, and **N12 → N13**, exhibit only small barriers in the range of 2.5−4.2 kcal/mol and are 40−60 kcal/mol exothermic. Interestingly, the ring closure involving two acetylene fragments (**N8 → N9** and **N12 → N13**) requires higher activation energy and is more exothermic than in the case of the ring closure between the acetylene fragment and the aromatic ring (**N4 → N5**). An almost twice-higher barrier height of 7.3 kcal/mol and a heat of reaction of −23.6 kcal/mol were calculated for the ring closure step in the Bittner−Howard naphthalene synthesis at the B3LYP/4-31G level.[49] This indicates that more accurate calculations may reduce the barrier and heat of reaction for the ring closure reactions in the HACA PAH synthesis. The ring closure steps are exothermic, and transition states **TS4^{II}**, **TS9^{II}**, and **TS13^{II}** exhibit an early character; the forming C−C bonds are almost 1 Å longer in **TS4^{II}** and **TS9^{II}** and almost 1.5 Å longer in **TS13^{II}** as compared to the regular C−C bond in phenanthrene. The structure and imaginary frequency of **TS13^{II}** indicate that this transition state corresponds to the rotation of the C_2H_3 fragment, which eventually leads to the ring closure involving two acetylene fragments. The same conclusion is valid for **TS10^{I}** calculated for the **B9 → B10** ring closure step in the phenanthrene synthesis from biphenyl (see above).

There are three hydrogen elimination steps in the considered network, **N3 → N6**, **N5 → P**, and **N13 → P**, which involve removal of an H atom from radical species, **N3**, **N5**, and **N13**, respectively. These reactions can proceed by two mechanisms, either by direct hydrogen loss or by hydrogen disproportionation. Although these steps are crucial both in the Bittner−Howard and Frenklach mechanisms of the PAH synthesis, it was unclear which pathway, i.e., the H disproportionation or direct H loss, is more favorable energetically. It should be noted that only the H loss channel was considered in the originally proposed

mechanisms[40−43] and no information was available so far concerning barrier heights and transition state structures for the H disproportionation reactions from radical intermediates in the PAH synthesis, except our earlier study of the $C_6H_5 + H \rightarrow C_6H_4 + H_2$ disproportionation.[50] The barriers of analogous reactions in the Frenklach and Bittner−Howard mechanisms of naphthalene formation have not been computed by Bauschlicher et al.[49] The geometries of singlet open-shell transition states **TS5b^{II}**, **TS6b^{II}**, and **TS14b^{II}** for the hydrogen abstraction channels could not be optimized using the UB3LYP method. On the other hand, for the direct H loss transition states **TS5a^{II}**, **TS6a^{II}**, and **TS14a^{II}** in the doublet electronic state, the UB3LYP optimization was successful. Instead of using DFT, we calculated **TS5b^{II}**, **TS6b^{II}**, and **TS14b^{II}** structures first at the UHF/6-31G* level, and then they were reoptimized using the CASSCF(4,6)/6-31G* method. The same method was applied for geometries of **N5**, **N3**, and **N13** in order to obtain barriers for the hydrogen disproportionation channels.

Similar to the biphenyl → phenanthrene reaction network, the H disproportionation mechanism is more favorable energetically for the **N3** → **N6**, **N5** → **P**, and **N13** → **P** reactions because the calculated barriers are 4.7, 0.9, and 0.7 kcal/mol, respectively, as compared to 40.2, 19.0, and 27.5 kcal/mol, respectively, for the unassisted hydrogen loss. The **N3** → **N6**, **N5** → **P**, and **N13** → **P** steps are found to be 67.4−92.5 kcal/mol exothermic and transition states **TS6b^{II}**, **TS5b^{II}**, and **TS14b^{II}** have an early character. It should be mentioned that the barrier for the $C_6H_5 + H \rightarrow o\text{-}C_6H_4 + H_2$ disproportionation reaction calculated at the higher G2M(cc,MP2)//CASSCF(10,10)/6-31G** level is somewhat higher, ∼9 kcal/mol, but the exothermicity of this reaction is lower, 29 kcal/mol.[50] On the other hand, the hydrogen loss **N3** → **N6**, **N5** → **P**, and **N13** → **P** reactions are endothermic by 36.0, 10.9, and 24.2 kcal/mol, respectively, and show late transition states **TS6a^{II}**, **TS5a^{II}**, and **TS14a^{II}**. The heats of the **N3** → **N6** and **N5** → **P** hydrogen loss channels are comparable with the values obtained by Bauschlicher at al.[49] for similar steps in the HACA naphthalene synthesis, 34.8 kcal/mol for the hydrogen loss from the $C_6H_5-C_2H_2$ radical (hydrogen elimination from the acetylene fragment) and 2.9 kcal/mol for the hydrogen loss from $C_{10}H_9$ (naphthalene with an 'extra' hydrogen). For the **N3** → **N6** hydrogen loss channel, we found a barrier of 40.2 kcal/mol and reaction endothermicity of 36.0 kcal/mol, which are almost the same as for the H elimination from $C_6H_5C_2H_2$ radical, leading to the production of phenylacetylene. Indeed, for the latter reaction, Yu et al.[47] found a barrier of 41.2 kcal/mol and reaction endothermicity of 38.2 kcal/mol using the BAC-MP4 method. Meanwhile, the hydrogen loss from the phenanthrene with an "extra" hydrogen in another position (in an external ring), **N13** → **P**, exhibits a higher endothermicity of 24.2 kcal/mol.

The **N3** → **N11** reaction represents a hydrogen atom transfer from the carbon atom of the aromatic ring and that of the side chain. A similar hydrogen migration process in the $C_6H_5-C_2H_2$ radical has been studied by Frenklach and co-workers[48] as a simplest example of hydrogen transfer in PAH molecules. They found the barrier height of 26.9 kcal/mol and the reaction energy of 0.7 kcal/mol for the hydrogen migration at the B3LYP/6-31G** level, which are very close to our B3LYP/6-31G* calculated values for the **N3** → **N11** case. Moreover, the values obtained at their best G2MP2 level (28.4 and 5.6 kcal/mol for the barrier height and reaction energy, respectively) are also similar with our estimates. This fact again confirms that the B3LYP method provides quite accurate barrier heights and reaction energies for reaction steps involved in the HACA PAH synthesis.

3. Reaction Rate Constants. Using the calculated reaction energetics and molecular parameters (shown in the Supporting Information), we can employ the transition state theory to compute rate constants at various temperatures. For the reactions which have a unimolecular character in the forward or reverse direction, the TST rates correspond to the high-pressure limit, whereas their pressure dependence can be evaluated using the RRKM theory, which is beyond the scope of this paper. Results are presented in Table 1. Table 2 shows equilibrium constants, which can be applied for calculations of reverse reaction steps. Although, to assess the competition among several reaction pathways, a kinetic simulation of the entire reaction network would be required, some comparisons can be made based on the calculated reaction rates.

Let us first compare the calculated rates with available experimental data. Arrhenius plots for various H abstraction reactions are shown in Figure 3a. The three-parameter fit of the hydrogen abstraction rates to the $k = AT^n \exp(-E_a/RT)$ expression (in cm^3 molecule^{-1} s^{-1}) gave the values of $5 \times 10^{-17}-3.7 \times 10^{-16}$ for A, 1.82−1.88 for n, and 9850−11320 for E_a (see Table 1). Among these reactions, **N1** + H → **N2** + H_2 with a barrier of 11.1 kcal/mol is the fastest, and **N10** + H → **N11** + H_2 with a barrier of 12.4 kcal/mol is the slowest one. The commonly used expression for hydrogen abstraction rate constants from aromatic species is $4.15 \times 10^{-10}\exp(-16000/RT)$ cm^3 molecule^{-1} s^{-1}.[38] As seen in Figure 3a, our computed values are in close agreement with the recommended rate coefficients for the temperature range between 500 and 3000 K. For instance, at 1500 K, the calculated rates for the **B5** + H → **B6** + H_2, **B8** + H → **B9** + H_2, and **N6** + H → **N7** + H_2 reactions are nearly identical with the recommended value, the **B1** + H → **B2** + H_2 and **N1** + H → **N2** + H_2 rates overestimate this value by factors of 4.4 and 6.5, respectively, and the **N10** + H → **N11** + H_2 rate underestimates it by a factor of 2.5. Considering that a single expression was recommended for various hydrogen abstraction reactions, the agreement of theoretical rate coefficients with experiment is satisfactory.

H disproportionation reactions where the H atom attacks an aromatic radical to produce H_2 are in general faster than hydrogen abstraction processes, because they show lower barriers, from 0.7 to 9.5 kcal/mol. In the fitted three-parameter expressions for the calculated rate constants (Table 1), A varies between 3×10^{-23} and 4×10^{-20}, n is in the 3.1−4.2 range, and E_a is spread between −1160 and 7190. To our knowledge, no experimental data are available for these types of reactions. Because of the high rate coefficients, the H disproportionation reactions are expected to play a significant role in PAH formation, although they have to compete with H addition to the radical site.

Figure 3b shows calculated rate constants for acetylene addition reactions. The reactions of C_2H_2 addition to aromatic radicals exhibit barriers of 1.8−4.5 kcal/mol. The **N2** + C_2H_2 → **N3** rate is computed to be the fastest in this group, whereas k(**N11** + C_2H_2 → **N12**) is the slowest. In the three-parameter expressions, A changes in the $8 \times 10^{-21}-4 \times 10^{-20}$ range, n is close to 2.5, and E_a varies between 1090 and 3650. Numerous experimental data are available for this type of reactions. In Figure 3b, we plotted rate constants measured for the C_6H_5 + C_2H_2 → $C_6H_5C_2H_2$ reaction by Wang and Frenklach[32] and by Lin and co-workers,[47] as well as for the **N3** + C_2H_2 → **N4** reaction[32] at 760 Torr. The rates are pressure-dependent and show a falloff behavior at $T > 1000$ K. Our calculations provide

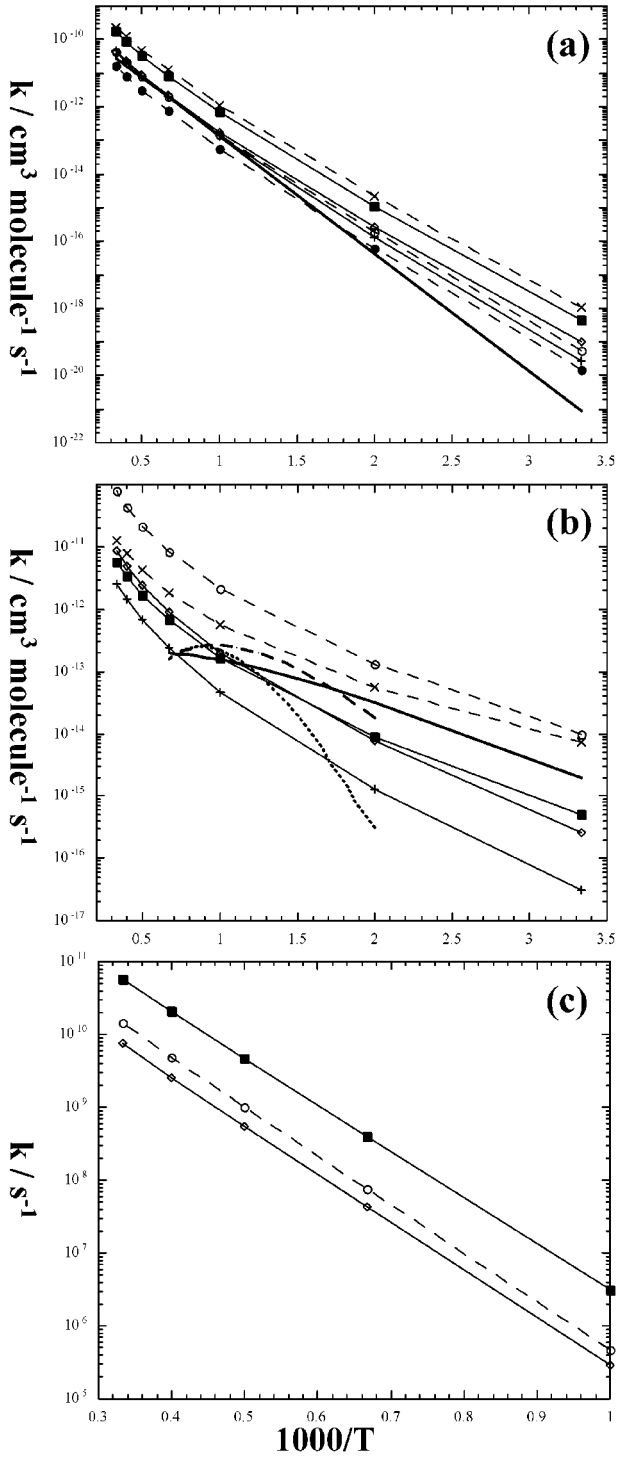

Figure 3. Arrhenius plots of calculated reaction rate constants (a) for hydrogen abstraction reactions, **B1** + H → **B2** + H_2 (solid square, solid line), **B5** + H → **B6** + H_2 (open circle, dashed line), **B8** + H → **B9** + H_2 (open diamond, solid line), **N1** + H → **N2** + H_2 (×, dashed line), **N6** + H → **N7** + H_2 (+, solid line), **N10** + H → **N11** + H_2 (solid circle, dashed line). Bold line shows recommended rate constants, 4.15×10^{-10} exp(−16000/*RT*) cm^3 molecule^{-1} s^{-1} (from ref 38). (b) For acetylene addition reactions, **B2** + C_2H_2 → **B3** (solid square, solid line), **N2** + C_2H_2 → **N3** (open circle, dashed line), **N3** + C_2H_2 → **N4** (open diamond, solid line), **N7** + C_2H_2 → **N8** (×, dashed line), **N11** + C_2H_2 → **N12** (+, solid line). Bold lines show experimental rate constants for the C_6H_5 + C_2H_2 → $C_6H_5C_2H_2$ reaction from refs 32 (dashed line) and 47 (solid line) and for **N3** + C_2H_2 → **N4** from ref 32 (dotted line). (c) For 1,4-H migration reactions, **N3**→**N11** (solid square, solid line) and $C_6H_5C_2H_2$→$C_6H_4C_2H_3$ from ref 48 calculated at the B3LYP/6-31G* (open circle, dashed line) and G2MP2 (diamond, solid line) levels of theory.

only a high-pressure limit. Nevertheless, the agreement with experiment is good at 1000 K for **B2** + C_2H_2 → **B3** and **N3** + C_2H_2 → **N4**, for which the calculated rates of $1.6-2.0 \times 10^{-13}$ cm^3 molecule^{-1} s^{-1} are close to the experimental values of $1.5-2.6 \times 10^{-13}$. Acetylene addition to biphenyl is a slow reaction because the barrier is high, ∼45 kcal/mol. The *A* factor and activation energy are fitted as 1.7×10^{-13} cm^3 molecule^{-1} s^{-1} and 47.0 kcal/mol, respectively. Even at $T > 1500$ K, the **B1** + C_2H_2 → **B11** rate constant is 4−7 orders of magnitude lower than those for acetylene additions to the radical species.

H elimination rate constants from radical intermediates are well fitted by two-parameter $k = A \exp(-E_a/RT)$ expressions (in s^{-1}). The rates show *A* factors in the $2.3 \times 10^{13}-4.3 \times 10^{14}$ range, and the activation energies E_a are close to the computed barriers varying between 17 and 41 kcal/mol. Molecular H_2 loss from **B11** to form phenanthrene is characterized by the 2.8×10^{12} *A* factor and ∼16 kcal/mol activation energy. The unimolecular reactions of ring closure are much faster, especially at $T < 1500$ K, because they have low activation energies, 1.2−5.3 kcal/mol. On the other hand, their *A* factors, in the $8.3 \times 10^{11}-5.0 \times 10^{12}$ range, are 1−3 orders of magnitude lower than those for the H elimination reactions. The rate coefficients for hydrogen migration, **B3** → **B9** and **N3** → **N11** are also well described by two-parameter expressions and have *A* factors of 1.6×10^{12} and 5.6×10^{12}, respectively. The former reaction corresponding to a 1,6-H shift is faster than the latter (1,4-H shift) because of the lower activation energy. The **N3** → **N11** reaction is analogous to hydrogen migration in the phenylethen-2-yl radical investigated by Frenklach and co-workers at various theoretical levels.[48] Both reactions exhibit similar barriers of 27−29 kcal/mol, and for the 1000−2500 K temperature range, the **N3** → **N11** high-pressure-limit rate coefficient is about 1 order of magnitude higher than those reported by Frenklach and co-workers[48] (see Figure 3c). Because the activation energies for the two reactions are close, the difference arises from the preexponential factors.

In the reaction network **I**, acetylene addition to **B1** (**B1** → **B11**) is much slower than the hydrogen abstraction (**B1** → **B2**) for the whole 300−3000 K temperature range. Therefore, the **B1** → **B11** → **P** reaction mechanism can contribute only if the concentration of H radicals is insignificant but that of C_2H_2 is high. If one considers unimolecular reactions of the key **B3** intermediate, the ring closure to **B4** is faster than the hydrogen migration to produce **B9** at all *T*, but at $T \geq 2000$ K, the difference in their rates is small. Ring closure of **B6** (**B6** → **B7**) is up to 3 times faster than **B3** → **B4**, especially at high temperatures. **B9** → **B10** is the fastest among the ring closure processes in the reaction network **I** since the corresponding barrier is only 1.0 kcal/mol. For hydrogen abstraction/disproportionation reactions, **B4** → **P** is always faster than **B3** → **B5**, **B5** → **B6**, and **B8** → **B9** but slower than **B10** → **P** at $T < 2500$ K.

In the naphthalene → phenanthrene synthesis, the reaction rates of **N3** with C_2H_2 are about 2 orders of magnitude lower than those for the **N3** → **N6** hydrogen disproportionation. The ring closure process along the reaction route R1 (**N4** → **N5**) is slower than those in R2 (**N8** → **N9**) and R3 (**N12** → **N13**) at $T \geq 1000$ K. On the other hand, a comparison of the hydrogen abstraction/disproportionation rates, **N5** → **P** in R1, **N6** → **N7** in R2, and **N10** → **N11** and **N13** → **P** (at $T \geq 1000$ K) in R3, show a preference of the reaction route R1. For the acetylene addition reactions, **N7** → **N8** in R2 has the fastest rate followed by **N3** → **N4** in R1 and **N11** → **N12** in R3. Certainly, a more detailed assessment of different reaction mechanisms can be

made only based on a detailed kinetic modeling of the entire reaction network taking into account the pressure dependence of reaction rate constants, which can be obtained from RRKM calculations.

IV. Conclusions

The results of density functional B3LYP and ab initio CASSCF calculations of the biphenyl → phenanthrene reaction network indicate that three reaction pathways, R1 (**B1** → **B2** → **B3** → **B4** → **P**), involving hydrogen atom abstraction from biphenyl followed by acetylene addition, ring closure, and hydrogen loss (disproportionation), R2 (**B3** → **B5** → **B6** → **B7** → **P**), where the acetylene addition to produce **B3** is followed by H loss (disproportionation), H abstraction, ring closure, and H addition, and R3 (**B3** → **B8** → **B9** → **B10** → **P**), where the formation of **B3** is followed by H addition and H abstraction (can be replaced by a 1,6-H shift), ring closure, and H loss (disproportionation), are competitive in the phenanthrene synthesis from biphenyl in the combustion of aromatic fuels according to the calculated energies and reaction rate constants. R1 exhibits lower barriers for the reaction steps **B3** → **B4** and **B4** → **P** following the formation of the radical intermediate **B3** and has a smaller number of steps than R2 and R3. However, the difference in barriers and heats of reactions for the R1−R3 routes is small, and kinetic modeling is required to determine actual contributions of these mechanisms in the PAH formation upon different conditions. Phenanthrene can be also produced in a two-step mechanism (route R4) by acetylene addition to biphenyl followed by elimination of molecular hydrogen. This process is less favorable energetically than R1−R3 because the barrier for the rate-determining step of C_2H_2 addition is as high as ∼45 kcal/mol. On the other hand, R4 can also contribute to the formation of phenanthrene from biphenyl in combustion, especially, at high temperatures and when the amount of free H radicals needed to carry on routes R1−R3 is insufficient.

Another interesting finding is that the reaction steps **B4** → **P**, **B3** → **B5** and **B10** → **P**, i.e., hydrogen elimination from radical intermediates **B3**, **B4**, and **B10**, can occur not only by direct hydrogen loss as it was proposed in the series of experimental works (see, for example, a recent review[33]) but also by the disproportionation mechanism. From our CASSCF calculations, barriers for the disproportionation channels are much lower than those for the hydrogen loss channels. Additionally, the disproportionation reactions are highly (>50 kcal/mol) exothermic, whereas the hydrogen loss reactions are 10−30 kcal/mol endothermic. The same conclusions can be made for the reaction steps **N5** → **P**, **N3** → **N6**, and **N13** → **P** in the naphthalene → phenanthrene reaction network. Meanwhile, one should remember that when a radical intermediate collides with a hydrogen atom, the disproportionation reaction has to compete with barrierless H addition to the radical site. In our previous study of the C_6H_5 + H reaction, we found that the disproportionation mechanism leading to *o*-C_6H_4 + H_2 takes over the recombination reaction to form C_6H_6 only at temperatures higher than 2000 K.[50] Nevertheless, the disproportionation pathways should be included into kinetic models of PAH formation in flames.

Route R1 (the Bittner−Howard mechanism) is also facile for the naphthalene → phenanthrene reaction network judging from the calculated reaction barriers. This mechanism involves H abstraction from naphthalene (**N1** → **N2**), acetylene addition (**N2** → **N3**), second acetylene addition to the first C_2H_2 fragment (**N3** → **N4**), and ring closure (**N4** → **N5**) and is completed by the H loss (disproportionation), **N5** → **P**. The other two reaction pathways starting from **N3**, namely, R2 (the Frenklach mechanism), H loss (disproportionation) followed by H abstraction, second acetylene addition to the aromatic ring, ring closure and completed by H addition, as well as R3 − H addition followed by H abstraction (which can be replaced by a 1,4-H migration), second acetylene addition to the aromatic ring, ring closure, and H loss (disproportionation), show somewhat higher barriers but have faster reaction rates for some individual steps and also can significantly contribute to the phenanthrene formation.

The calculations demonstrate that the HACA scheme provides viable mechanisms for the PAH formation and growth in flames. On the other hand, a new mechanism is suggested for the formation of three fused aromatic rings (phenanthrene-like structures) from biphenyl-like precursors. This pathway does not require a presence of H radicals and involves acetylene addition between two aromatic rings followed by H_2 elimination. Although the highest barrier for this reaction is about 45 kcal/mol, it can take place in high-temperature combustion. The reaction rate constants and equilibrium constants obtained in the present study should facilitate kinetic simulation of various mechanisms of the PAH formation.

Acknowledgment. This work was supported by the Petroleum Research Fund of ROC, Academia Sinica, and the National Science Council of ROC under Grant NSC 9002113-M-001-068.

Supporting Information Available: B3LYP/6-31G* optimized geometries for all species involved in the considered networks, total energies of the reactants and products, harmonic frequencies, zero-point energy corrections, and moments of inertia for all structures calculated at the B3LYP/6-31G* level. This material is available free of charge via the Internet at http://pubs.acs.org.

References and Notes

(1) Grimmer, G. *Environmental Carcinogens: Polycyclic Aromatic Hydrocarbons: Chemistry, Occurrence, Biochemistry, Carcinogenity*; CRC Press: Boca Raton, FL, 1983.

(2) Ramdahl, T.; Bjorseth, J. *Handbook of Polycyclic Aromatic Hydrocarbons*, 2nd ed.; Marcel Dekker: New York, 1985; p 1.

(3) Dias, J. R. *Handbook of Polycyclic Hydrocarbons*; Elsevier: Amsterdam, 1987.

(4) Siegmann, K.; Siegmann, H. C. In *Molecular precursor of soot and quantification of the associated health risk. In Current problems in condensed matter*; Moran-Lopez, Ed.; Plenum Press: New York, 1998; p 143.

(5) Venkataraman, C.; Friedlander, S. K. *Environ. Sci. Technol.* **1994**, *28*, 563.

(6) Allen, J. O.; Dookeran, K. M.; Smith, K. A.; Sarofim, A. F.; Taghizadeh, K.; Lafleur, A. L. *Environ. Sci. Technol.* **1996**, *30*, 1023.

(7) Westerholm, R. N.; Almen, J.; Li, H.; Rannug, J. U.; Egeback, K. E.; Gragg, K. *Environ. Sci. Technol.* **1991**, *25*, 332.

(8) Rogge, W. F.; Hildemann, L. M.; Mazurek, M. A.; Cass, G. R.; Simoneit, B. R. T. *Environ. Sci. Technol.* **1993**, *27*, 636.

(9) Lowenthal, D. H.; Zielinska, B.; Chow, J. C.; Watson, J. G.; Gautam, M.; Ferguson, D. H.; Neuroth, G. R.; Stevens, K. D. *Atmos. Environ.* **1994**, *28*, 731.

(10) Nielsen, T. *Atmos. Environ.* **1996**, *30*, 3481.

(11) Kamens, R. M.; Coe, D. L. *Environ. Sci. Technol.* **1997**, *31*, 4.

(12) Pisupati, S. V.; Wasco, R. S. *Abstr. Papers Am. Chem. Soc.* **1998**, *216*, 049-ENVR.

(13) Revuelta, C. C.; Santiago, E. D.; Vazquez, J. A. R. *Environ. Technol.* **1999**, *20*, 61.

(14) Doskey, P. V.; Talbot, T. W. *Limnol. Oceanogr.* **2000**, *45*, 895.

(15) Ramdahl, T. *Nature (London)* **1983**, *306*, 580.

(16) Atal, A.; Levendis, Y. A.; Carlson, J.; Dunayevskiy, Y.; Vouros, P. *Combust. Flame.* **1997**, *110*, 17.

(17) Gundel, L. A.; Lee, V. C.; Mahanama, K. R. R.; Stevens, R. K. *Atmos. Environ.* **1995**, *29*, 1719.

(18) Perera, F. P.; Jedrychowski, W.; Rauh, V.; Whyatt, R. M. *Environ. Health Perspect.* **1999**, *107*, 451.

(19) Rodgman, A.; Smith, C. J.; Perfetti, T. A. *Human Exp. Toxicol.* **2000**, *19*, 573.
(20) Levendis, Y. A.; Atal, A.; Carlson, J. B.; Quintana, M. D. *Chemosphere* **2001**, *42*, 775.
(21) Levendis, Y. A.; Atal, A.; Carlson, J. B. *Combust. Sci. Technol.* **1998**, *134*, 407.
(22) Meharg, A. A.; Wright, J.; Dyke, H.; Osborn, D. *Environ. Pollut.* **1998**, *99*, 29.
(23) Panagiotou, T.; Levendis, Y. A.; Carlson, J.; Dunayevskiy, Y. M.; Vouros, P. *Combust. Sci. Technol.* **1996**, *116*, 91.
(24) Cecinato, A.; Ciccioli, P.; Brancaleoni, E.; Brachetti, A.; Zagari, M.; Vasconcellos, P. D. *Ann. Chim. (Rome)* **1997**, *87*, 555.
(25) Page, D. S.; Boehm, P. D.; Douglas, G. S.; Bence, A. E.; Burns, W. A.; Mankiewicz, P. J. *Marine Pollut. Bull.* **1999**, *38*, 247.
(26) Muraleedharan, T. R.; Radojevic, M.; Waugh, A.; Caruana, A. *Atmos. Environ.* **2000**, *34*, 3033.
(27) Frenklach, M.; Warnatz, J. *Combust. Sci. Technol.* **1987**, *51*, 265.
(28) Haynes, B. S. In *Fossil Fuel Combustion*; Bartok, W., Sarofim, A. F., Eds.; John Wiley and Sons: New York, 1991; p 261.
(29) Smedley, J. M.; Williams, A.; Bartle, K. D. *Combust. Flame* **1992**, *91*, 71.
(30) Ladommatos, N.; Rubenstein, P.; Harrison, K.; Xiao, Z.; Zhao, H. *J. I. Energy* **1997**, *70*, 84.
(31) McEnally, C. S.; Pfefferle, L. D. *Combust. Sci. Technol.* **1997**, *128*, 257.
(32) Wang, H.; Frenklach, M. *Combust. Flame* **1997**, *110*, 173.
(33) Richter, H.; Howard, J. B. *Prog. Energy Combust. Sci.* **2000**, *26*, 565.
(34) Gerhardt, Ph.; Loffler, K. H.; Homann, K. H. *Chem. Phys. Lett.* **1987**, *137*, 306.
(35) Howard, J. B.; McKinnon, J. T.; Makarovsky, Y.; Lafleur, A. L.; Johnson, M. E. *Nature* **1991**, *352*, 139.
(36) Howard, J. B.; Das Chowdhury, K.; Vander Sande, J. B. *Nature* **1994**, *370*, 603.
(37) Richter, H.; Hernadi, K.; Caudano, R.; Fonseca, A.; Migeon, H.-N.; Nagy, B. J.; Schneider, S.; Vandooren, J.; Van Tiggelen, P. J. *Carbon* **1996**, *34*, 427.
(38) Richter, H.; Grieco, W. J.; Howard, J. B. *Combust. Flame* **1999**, *119*, 1.
(39) Lafleur, A. L.; Howard, J. B.; Taghizadeh, K.; Plummer, E. F.; Scott, L. T.; Necula, A.; Swallow, K. C. *J. Phys. Chem.* **1996**, *100*, 17421.
(40) Wang, H.; Frenklach, M. *Combust. Flame* **1997**, *110*, 173.
(41) Frenklach, M.; Clary, D. W.; Gardiner, W. C.; Stein, S. E. *Symp. (Int.) Combust. [Proc.], 20th* **1984**, 887.
(42) Wang, H.; Frenklach, M. *J. Phys. Chem.* **1994**, *98*, 11465.
(43) Appel, J.; Bockhorn, H.; Frenklach, M. *Combust. Flame* **2000**, *121*, 122.
(44) Bittner, J. D.; Howard, J. B. *Symp. (Int.) Combust. [Proc.], 18th* **1981**, 1105.
(45) Frenklach, M.; Clary, D. W.; Gardiner, W. C.; Stein, S. E. *Symp. (Int.) Combust. [Proc.], 21st* **1986**, 1067.
(46) Mebel, A. M.; Lin, M. C.; Yu, T.; Morokuma, K. *J. Phys. Chem. A* **1997**, *101*, 3189.
(47) Yu, T.; Lin, M. C.; Melius, C. F. *Int. J. Chem. Kinet.* **1994**, *26*, 1095.
(48) (a) Moriarty, N. W.; Brown, N. J.; Frenklach, M. *J. Phys. Chem. A* **1999**, *103*, 7127. (b) Frenklach, M.; Moriarty, N. W.; Brown, N. J. *Symp. (Int.) Combust. [Proc.], 27th* **1998**, 1655.
(49) Bauschlicher, C. W.; Ricca, A. *Chem. Phys. Lett.* **2000**, *326*, 283.
(50) Mebel, A. M.; Lin, M. C.; Chakraborty, D.; Park, J.; Lin, S. H.; Lee Y. T. *J. Chem. Phys.* **2001**, *114*, 8421.
(51) Melius, C. F.; Colvin, M. E.; Marinov, N. M.; Pitz, W. J.; Senkan, S. M. *Symp. (Int.) Combust. [Proc.], 26th* **1996**, 685.
(52) (a) Becke, A. D. *J. Chem. Phys.* **1992**, *96*, 2155. (b) Becke, A. D. *J. Chem. Phys.* **1992**, *97*, 9173. Becke, A. D. *J. Chem. Phys.* **1993**, *98*, 5648.
(53) Lee, C.; Yang, W.; Parr, R. G. *Phys. Rev.* **1988**, *B37*, 785.
(54) Hehre, W. J.; Ditchfield, R.; Pople, J. A. *J. Chem. Phys.* **1972**, *56*, 2257.
(55) (a) Schlegel, H. B.; Robb, M. A. *Chem. Phys. Lett.* **1982**, *93*, 43. (b) Bernardi, F.; Bottini, A.; McDougall, J. J. W.; Robb, M. A.; Schlegel, H. B. *Far. Symp. Chem. Soc.* **1984**, *19*, 137. (c) Frisch, M. J.; Ragazos, I. N.; Robb, M. A.; Schlegel, H. B. *Chem. Phys. Lett.* **1992**, *189*, 524. (d) Yamamoto, N.; Vreven, T.; Robb, M. A.; Frisch, M. J.; Schlegel, H. B. *Chem. Phys. Lett.* **1996**, *250*, 373.
(56) Frisch, M. J.; Trucks, G. W.; Schlegel, H. B.; Scuseria, G. E.; Robb, M. A.; Cheeseman, J. R.; Zakrzewski, V. G.; Montgomery, J. A., Jr.; Stratmann, R. E.; Burant, J. C.; Dapprich, S.; Millam, J. M.; Daniels, A. D.; Kudin, K. N.; Strain, M. C.; Farkas, O.; Tomasi, J.; Barone, V.; Cossi, M.; Cammi, R.; Mennucci, B.; Pomelli, C.; Adamo, C.; Clifford, S.; Ochterski, J.; Petersson, G. A.; Ayala, P. Y.; Cui, Q.; Morokuma, K.; Malick, D. K.; Rabuck, A. D.; Raghavachari, K.; Foresman, J. B.; Cioslowski, J.; Ortiz, J. V.; Stefanov, B. B.; Liu, G.; Liashenko, A.; Piskorz, P.; Komaromi, I.; Gomperts, R.; Martin, R. L.; Fox, D. J.; Keith, T.; Al-Laham, M. A.; Peng, C. Y.; Nanayakkara, A.; Gonzalez, C.; Challacombe, M.; Gill, P. M. W.; Johnson, B. G.; Chen, W.; Wong, M. W.; Andres, J. L.; Head-Gordon, M.; Replogle, E. S.; Pople, J. A. *Gaussian 98*, revision A.7; Gaussian, Inc.: Pittsburgh, PA, 1998.
(57) Glasstone, S.; Laidler, K. J.; Eyring, H. *The Theory of Rate Processes*; McGraw-Hill: New York, 1941.
(58) Steinfield, J.; Francisco, J.; Hase, W. *Chemical Kinetics and Dynamics*; Prentice-Hall: Englewood Cliffs, NJ, 1989.
(59) Froese, R. D. J.; Coxon, J. M.; West, S. C.; Morokuma, K. *J. Org. Chem.* **1997**, *62*, 6991.